



## Original article

# Docking studies of benzylidene anabaseine interactions with $\alpha 7$ nicotinic acetylcholine receptor (nAChR) and acetylcholine binding proteins (AChBPs): Application to the design of related $\alpha 7$ selective ligands

David C. Kombo<sup>a,\*</sup>, Anatoly Mazurov<sup>a</sup>, Kartik Tallapragada<sup>a</sup>, Philip S. Hammond<sup>a</sup>, Joseph Chewning<sup>a</sup>, Terry A. Hauser<sup>a</sup>, Montserrat Vasquez-Valdivieso<sup>b</sup>, Daniel Yohannes<sup>a</sup>, Todd T. Talley<sup>c</sup>, Palmer Taylor<sup>c</sup>, William S. Caldwell<sup>a</sup>

<sup>a</sup> Targacept Inc., Molecular Design, 200 East First Street, Suite 300, Winston-Salem, NC 27101-4165, USA

<sup>b</sup> University of Edinburgh, Structural Biochemistry Group, Mayfield Rd, Edinburgh EH9 3JR, Scotland, UK

<sup>c</sup> Department of Pharmacology, Skaggs School of Pharmacy and Pharmaceutical Sciences, University of California, San Diego, La Jolla, CA 92093-0657, USA

## ARTICLE INFO

## Article history:

Received 10 August 2011

Received in revised form

17 September 2011

Accepted 20 September 2011

Available online 29 September 2011

## Keywords:

AChBPs

Nicotinic acetylcholine receptor  $\alpha 7$

Docking

Benzylidene-anabaseine analogs

Spirodiazepine and spiroimidazoline quinuclidine series

## ABSTRACT

AChBPs isolated from *Lymnaea stagnalis* (Ls), *Aplysia californica* (Ac) and *Bulinus truncatus* (Bt) have been extensively used as structural prototypes to understand the molecular mechanisms that underlie ligand-interactions with nAChRs [1]. Here, we describe docking studies on interactions of benzylidene anabaseine analogs with AChBPs and  $\alpha 7$  nAChR. Results reveal that docking of these compounds using Glide software accurately reproduces experimentally-observed binding modes of DMXBA and of its active metabolite, in the binding pocket of Ac. In addition to the well-known nicotinic pharmacophore (positive charge, hydrogen-bond acceptor, and hydrophobic aromatic groups), a hydrogen-bond donor feature contributes to binding of these compounds to Ac, Bt, and the  $\alpha 7$  nAChR. This is consistent with benzylidene anabaseine analogs with OH and NH<sub>2</sub> functional groups showing the highest binding affinity of these congeners, and the position of the ligand shown in previous X-ray crystallographic studies of ligand-Ac complexes. In the predicted ligand-Ls complex, by contrast, the ligand OH group acts as hydrogen-bond acceptor. We have applied our structural findings to optimizing the design of novel spirodiazepine and spiroimidazoline quinuclidine series. Binding and functional studies revealed that these hydrogen-bond donor containing compounds exhibit improved affinity and selectivity for the  $\alpha 7$  nAChR subtype and demonstrate partial agonism. The gain in affinity is also due to conformational restriction, tighter hydrophobic enclosures, and stronger cation- $\pi$  interactions. The use of AChBPs structure as a surrogate to predict binding affinity to  $\alpha 7$  nAChR has also been investigated. On the whole, we found that molecular docking into Ls binding site generally scores better than when a  $\alpha 7$  homology model, Bt or Ac crystal structure is used.

© 2011 Elsevier Masson SAS. All rights reserved.

**Abbreviations:** Ac, *Aplysia californica*; AChBP, Acetylcholine-binding protein; AD, Alzheimer's disease; ADHD, Attention deficit hyperactivity disorder; BA, Benzylidene anabaseine; Bt, *Bulinus truncatus*; CDS, Cognitive dysfunction in schizophrenia; CNS, Central nervous system; DMXBA, 3-(2,4-dimethoxybenzylidene)-anabaseine; HBD, Hydrogen-bond donor; Ls, *Lymnaea stagnalis*; nAChR, Nicotinic acetylcholine receptor; PD, Parkinson's disease; Pdb, Protein databank; QPLD, QM-polarized ligand docking; rmsd, Root-mean-squared-deviation; ROC, Receiver operating characteristic curve; SP, Standard precision; XP, Extra precision.

\* Corresponding author. Tel.: +1 336 480 2127; fax: +1 336 480 2107.

E-mail address: david.kombo@targacept.com (D.C. Kombo).

## 1. Introduction

nAChRs are members of the Cys-Loop ligand-gated ion channel superfamily, located both in the peripheral and central nervous systems. These receptors, existing as both homopentameric and heteropentameric transmembrane ion channels, are validated therapeutic targets for various CNS pathologies (for reviews of nAChRs as targets for drug discovery, see Romanelli et al. [1], Breining [2], Schmitt [3], Conejero-Goldberg et al. [4], Mazurov et al. [5], Daly [6], and Taly et al. [7]). Examples of disease indications under active investigation include Alzheimer's disease (AD) and Parkinson's disease (PD), cognitive dysfunction in Schizophrenia (CDS), addiction disorders, attention deficit hyperactivity

disorder (ADHD), age-associated memory impairment (AAMI), pain management, anxiety, depression and inflammation-mediated processes. A number of compounds targeting nAChRs and representing a wide variety of pharmacologic actions are in advanced clinical trials or on the market.

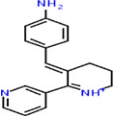
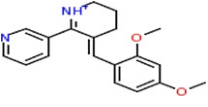
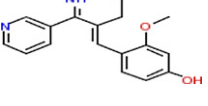
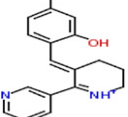
Chantix<sup>®</sup>, a partial agonist at  $\alpha 4\beta 2$  and a full agonist at  $\alpha 7$  nAChR from Pfizer, has recently been launched for smoking cessation [8,9]. ABT-089, a selective nAChR agonist from Abbot, completed Phase II clinical trials for ADHD and AD but was not advanced further. ABT-894, an nAChR agonist discovered by Abbot in collaboration with NeuroSearch, completed three Phase II clinical trials in 2008 for ADHD and diabetic neuropathic pain. AZD-3480, an  $\alpha 4\beta 2$  selective partial agonist, showed positive results in Phase 2 trials for AAMI and ADHD. One of the anabaseine analogs under study in this work, GTS-21 (DMXBA or compound **2** in Table 1) has been investigated in clinical trials for ADHD (completed), AD (completed), and inflammation (ongoing) [10]. Finally, TC-5619, an  $\alpha 7$  selective modulator, has shown positive top-line results from a Phase 2 clinical proof of concept trial to assess it as an augmentation therapy to improve cognition in patients with schizophrenia [11]. Understanding the molecular basis for the binding and selectivity of nAChR ligands that interact with this protein superfamily would be an important step toward designing better drugs against these targets.

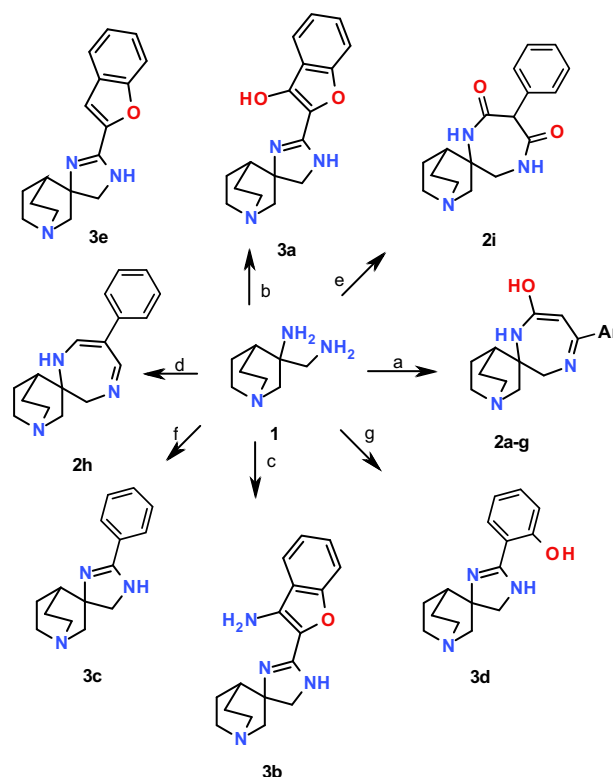
AChBP is a homopentamer similar in structure to the extracellular ligand-binding domain of nAChRs. The availability of several crystal structures of AChBPs, both free and/or in complex with various nicotinic ligands, has provided much needed information regarding the protein-ligand molecular recognition process [12–17]. These and additional studies have provided data indicating that ligand-nAChR interactions are characterized by cation- $\pi$  interactions, hydrogen-bonding between the typical cationic center of secondary and tertiary amine containing nAChR ligands and the protein backbone, receptor loop C flexibility, water-mediated and hydrophobic interactions, and capacity to accommodate ligands of differing structure at the binding site at the interface of two subunits [18–20]. Successful results have recently been reported using an AChBP crystal structure as a template for molecular docking, to identify novel  $\alpha 7$  nAChR ligands through screening of

a proprietary compound collection [21]. Three-dimensional structures of AChBP have also been used as templates to rationalize agonists binding to the homologous homopentameric  $\alpha 7$  nAChR [17]. Thus, the homologous AChBPs and associated co-crystal structures with nAChR ligands provide a rich starting point for understanding interactions for the various nAChR subtypes.

Benzylidene derivatives of the alkaloid anabaseine, are known for their functional selectivity toward  $\alpha 7$  nicotinic receptors [22,23]. A set of these compounds has been studied extensively with regards to their dissociation constants (Table 1) for the AChBPs from Ls, Ac, and Bt [24]. It was found that the 4-hydroxy benzylidene anabaseine compounds are among the most potent ligands in the series. Spectroscopic studies were able to ascertain the ionization state of 4-hydroxy substituted and un-substituted benzylidene anabaseine compounds. Binding studies of benzylidene anabaseine analogs with rat  $\alpha 7$  and  $\alpha 4\beta 2$  have also been reported more recently [25]. Recent crystallographic studies of the 4-hydroxy metabolite of 3-(2,4-dimethoxybenzylidene)-anabaseine in complexation with *Aplysia* AChBP have shown that its OH group donates a hydrogen-bond to a polar side-chain triad of Asp-164, Ser-166 and Ser-167 in loop F [17]. These findings provided us

**Table 1**  
2D structure of benzylidene anabaseine analogs and their dissociation constants with AChBPs isolated from Ls, Ac and Bt [24].

Structures	Name	Ls Kd (nM)	Ac Kd (nM)	Bt Kd (nM)
	<b>1</b>	0.8	3	33
	<b>2</b>	19	330	59
	<b>3</b>	0.4	3	22
	<b>4</b>	0.8	6	93



**Scheme 1.** Synthesis of  $\alpha 7$  nAChR ligands. Reagents and conditions: (a) ArCOCH<sub>2</sub>-CO<sub>2</sub>Me, *i*-BuOH, 100 °C, overnight; (b) methyl 2-(cyanomethoxy)benzoate, CS<sub>2</sub> (one drop), 100–110 °C, overnight; (c) (2-cyanophenoxy)acetone, CS<sub>2</sub> (one drop), 100–110 °C, overnight; (d) [3-(dimethylamino)-2-phenylprop-2-enylidene]-dimethylammonium hexafluorophosphate, MeOH, reflux, overnight; (e) diethyl 2-phenylmalonate, 150 °C, 5 min; (f) methyl benzimidate hydrochloride, methanol, 150 °C (microwave), 5 min; (g) 4-hydroxycoumarin, *t*-butanol, 100 °C, overnight. Compounds containing hydroxyl group (**2a–g**, **3a**) or amino group (**3b**) as a hydrogen bond donor have been synthesized by coupling 3-amino-3-(aminomethyl)quinuclidine (**1**) with series of aroylacetates [27], methyl 2-(cyanomethoxy)benzoate or (2-cyanophenoxy)acetone. Spirodiazepine **2h** without hydroxyl moiety has been obtained by condensation of diamine **1** with [3-(dimethylamino)-2-phenylprop-2-enylidene]-dimethylammonium hexafluorophosphate. Heating in a microwave of diamine **1** with diethyl 2-phenylmalonate or methyl benzimidate provided 1,4-diazepindione **2i** and phenylimidazoline **3c**. Hydroxyphenylimidazoline **3d** has been carried out by cyclization of 3-amino-3-(aminomethyl)quinuclidine (**1**) with 2-(2-hydroxyphenyl)-1,3-benzoxazin-4-one.

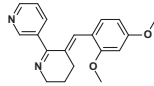
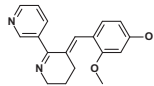
**Table 2**

nAChR competitive binding: Percent inhibition ( $\pm$ standard error) of control radioligand binding to nAChRs of the designed spirodiazepine and spiroimidazole quinuclidines tested at 5  $\mu$ M in radioactive displacement assays. Values in parentheses represent  $K_i$  values in nM. The  $\alpha 7$  radioligand [ $^3$ H]-methyllycaonitine was used for  $\alpha 7$  binding studies on rat hippocampal membranes and the nicotinic radioligand [ $^3$ H]-epibatidine was used for binding studies at  $\alpha 4\beta 2$  on rat cortical membranes, ganglion-type nicotinic receptors on SH-SY5Y cellular membranes and muscle-type nicotinic receptors on TE-671 cellular membranes. See [Experimental Section](#) for details. NT = not tested. For comparison purpose, corresponding data for compounds **2** and **3** of Table 1 are also shown.

Compound	Structure	$\alpha 7$	$\alpha 4\beta 2$	$\alpha 3\beta 4$	$\alpha 1\beta\gamma\delta$
<b>2a</b>		95 $\pm$ 3 (140 $\pm$ 7)	15 $\pm$ 1	NT	NT
<b>2b</b>		87 $\pm$ 3 (110)	7 $\pm$ 1	NT	NT
<b>2c</b>		93 $\pm$ 7 (87)	12 $\pm$ 1	NT	NT
<b>2d</b>		98 $\pm$ 3 (42)	42 $\pm$ 14	63 $\pm$ 0.4	38 $\pm$ 5
<b>2e</b>		95 $\pm$ 3 (77)	62 $\pm$ 15	89 $\pm$ 0.45	28 $\pm$ 6
<b>2f</b>		98 $\pm$ 2 (58)	20 $\pm$ 1	NT	NT
<b>2g</b>		84 $\pm$ 4 (150)	14 $\pm$ 3	NT	NT
<b>2h</b>		27 $\pm$ 5	6 $\pm$ 2	NT	NT
<b>2i</b>		19 $\pm$ 1	2 $\pm$ 1	NT	NT
<b>3a</b>		93 $\pm$ 6 (7.2 $\pm$ 3)	32 $\pm$ 11	55 $\pm$ 3	15 $\pm$ 10
<b>3b</b>		96 $\pm$ 1 (120)	9 $\pm$ 1	47 $\pm$ 3	38 $\pm$ 2
<b>3c</b>		1 $\pm$ 9	11 $\pm$ 2	NT	NT
<b>3d</b>		77 $\pm$ 3 (290)	4 $\pm$ 1	NT	NT
<b>3e</b>		33 $\pm$ 3	4 $\pm$ 2	13 $\pm$ 1	26 $\pm$ 5

(continued on next page)

Table 2 (continued)

Compound	Structure	$\alpha 7$	$\alpha 4\beta 2$	$\alpha 3\beta 4$	$\alpha 1\beta\gamma\delta$
2		(1300 ± 550)	(51 ± 10)	(2500 ± 270)	(3900 ± 770)
3		106 ± 3 (420)	97 ± 1 (19 ± 6)	75 ± 1 (970 ± 110)	72 ± 3

with a starting point for modeling studies aimed at deciphering the structural features that drive the binding affinity of these nAChR ligands. Using molecular docking, and homology modeling studies, we found that a similar hydrogen-bond donor feature contributes to the interaction with *Bulinus* AChBP and the  $\alpha 7$  nAChR as well. In the case of *Lymnaea*, however, the F-loop region appears not to participate to such hydrogen-bond interaction. Instead, the ligand OH group accepts a hydrogen bond from an amino acid side-chain located in a different region of the binding site. Targeting the  $\alpha 7$  subtype of neuronal nicotinic acetylcholine receptor, we have designed related hydrogen-bond donor containing spirodiazepines and spiroimidazolines quinuclidine series (Scheme 1). We find that these compounds selectively bind to the  $\alpha 7$  receptor with  $K_i$  in the low nanomolar range.

## 2. Results

### 2.1. Molecular docking of benzylidene anabaseine analogs

Validation of the docking procedure for AChBP was carried out by self-docking compounds **2** and compounds **3** co-crystallized with Ac [17], as described in supporting information (S1, Table S1, Figs. S1, S2 and S3). Table S1 illustrate that conformational

restriction, hydrophobic enclosures, and cations- $\pi$  interactions also contribute to the binding free energy of benzylidene anabaseine, in addition to the more common van der Waals, coulombic, lipophilic and hydrogen-bond interactions (data not shown). Compounds **1** and **3** exhibit the strongest binding affinities (Table 1) to the Ac protein. While the crystal structure of compound **3** in complex with Ac has been solved, no such data are available for compound **1**. Docking of **1** into the Ac binding site (Fig. 1), suggests that compound **1** exhibits strikingly similar interactions to those crystallographically-observed for the Ac-compound **3** complex, including the bifurcated HB donation to the whole amino acid triad Asp-164, Ser-166 and Ser-167 (see also Fig. S3 herein and Fig. 4 of Hibbs et al. [17]).

As shown in Fig. 2, docking compound **3** in the Bt protein (pdb code: 2BJ0, resolution 2.0 Å) also results in a similar hydrogen-bonding pattern: the protonated nitrogen atom makes a hydrogen bond with the backbone carbonyl oxygen atom of Trp-142, the nitrogen atom of the pyridine ring makes a hydrogen-bond with the backbone NH group of Val-113, while the ligand OH group donates a hydrogen-bond to the hydroxyl group of Tyr-164, a residue located in the F-loop region of the protein. Given the presence of Glu-163 within hydrogen-bond forming distance of this region, it is possible that an alternate conformation might include

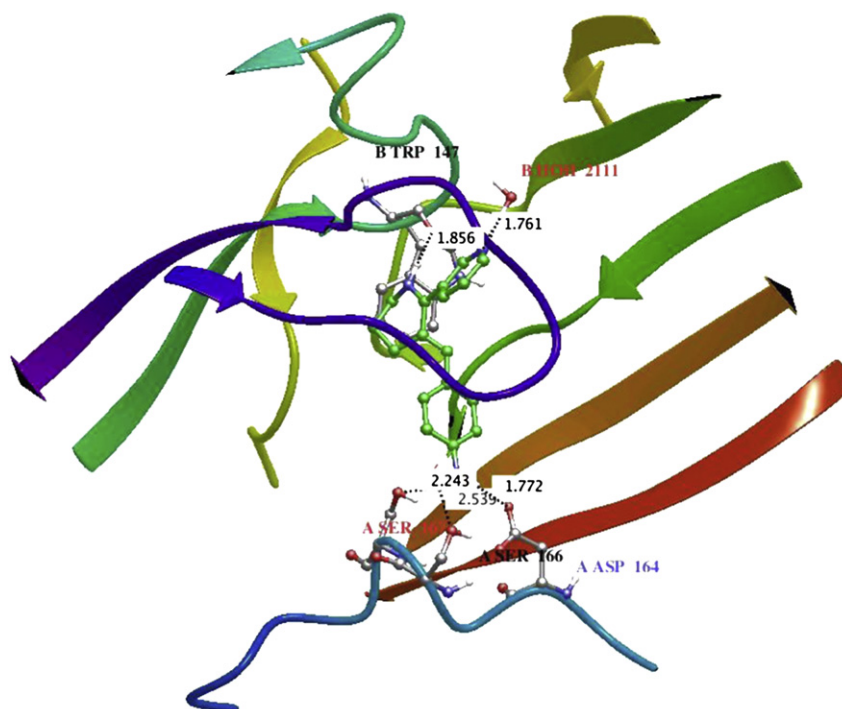
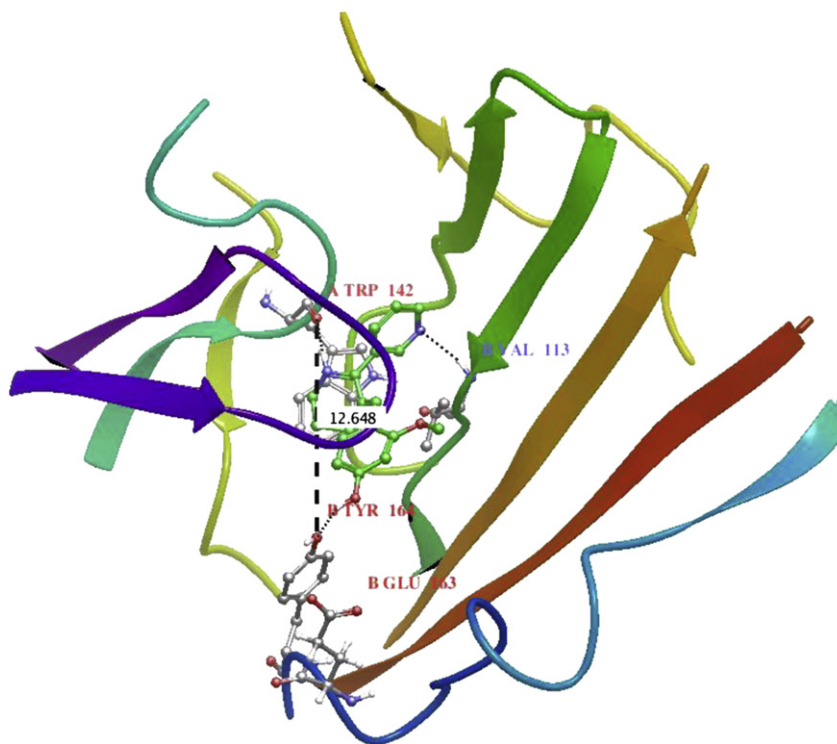


Fig. 1. Compound **1** docked into Ac: note the NH<sub>2</sub> group hydrogen bond with Ser-166, Ser-167 & Asp-164 in the complementary face, in a manner reminiscent of compound **3** pose in Ac crystal structure.



**Fig. 2.** Binding mode of compound **3** in the binding site of Bt protein. The OH group of the ligand donates a hydrogen-bond to Tyr-164 of the complementary face. The pyridine N atom makes an H-bond with the NH group of Val-113 in the complementary face, while the cationic center hydrogen bonds to Trp-142 backbone carbonyl group. The F-loop is shown in dark blue. Also shown is the distance (12.6 Å) between the backbone oxygen atom of Trp-142 and side-chain oxygen atom of Tyr-164.

the ligand hydroxyl group being involved in a bifurcated hydrogen bond donation to Tyr-164, and Glu-163.

In the case of Ls, however, the ligand hydroxyl group at position 4 accepts a hydrogen-bond from the side-chain carbamoyl hydrogen of Gln-73 of the complementary face, while the methoxy

group accepts a hydrogen-bond from the side-chain of Tyr-192 of the principal face, as shown in Fig. 3. Compared to its orientation in Ac and Bt binding sites, it appears as though the ligand has kept its quintessential hydrogen bond between the protonated ligand and the carbonyl oxygen atom of the conserved Trp-143, but has made

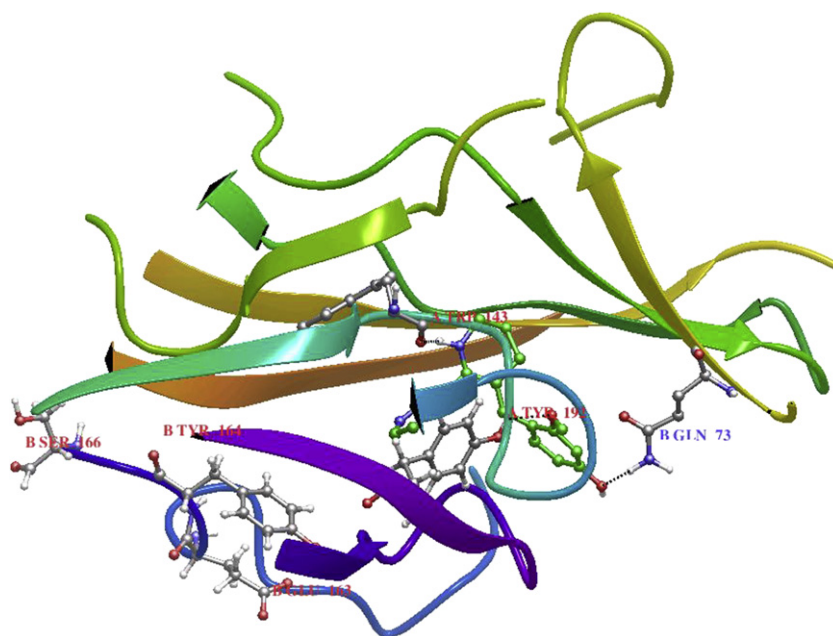


**Fig. 3.** Compound **3** docked into Ls: Ligand OH group accepts an HB from Gln-73 of the complementary face, while its methoxy group accepts an HB with Tyr-192 of the principal face. The cationic center donates to the backbone carbonyl group of Trp-143, in the principal face. The ligand makes a 90° rotation compared to its orientation in Ac and Bt binding sites. The amino acid side-chains which directly interact with the ligand and those of the F-loop that could have interacted with the ligand like in Ac and Bt are shown in ball and stick.

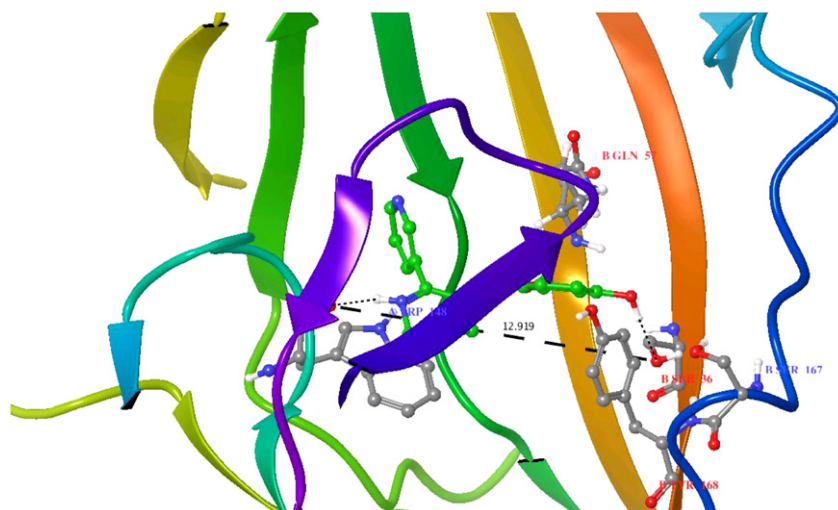


**Fig. 4.** Compound **3** (in green) docked into rat  $\alpha 7$  homology model. The ligand OH group donates a Hydrogen-bond to Ser-36 (in the complementary face), which is located in the neighborhood of Tyr-168, and Ser-167 in the F-loop (shown in dark blue). The cationic center donates a hydrogen bond to the backbone CO group of Trp-148, in the principal face. Also shown are the distance between the backbone oxygen atom of Trp-148 and side-chain oxygen atom of Ser-36, and Gln-57 (in the complementary face).

a 90° rotation, thereby allowing its OH and methoxy group to interact with Gln-73 and Tyr-192, respectively. Likewise, OH group at position 4 of compound **4**, which is among the most potent in binding to Ls, also accepts a hydrogen-bond from Gln-73 of the complementary face, while its OH group at position 2 donates a hydrogen-bond to the OH group of Tyr-192 of the principal face, as shown in Fig. S4.

The three-dimensional structure of the  $\alpha 7$  nAChR was derived by homology modeling, as described in the methods section. Biochemical validation of the  $\alpha 7$  homology model was carried out by docking a diverse chemical library of 493 compounds of known binding affinity to the  $\alpha 7$  receptor. The procedure used and results obtained are described in Supplemental information S2. In summary, a Roc score of 0.74 was achieved, which is much better than 0.53, the corresponding value obtained when one uses the experimentally-observed crystal structure of Ac as a surrogate, as shown in Table 3. The hydrogen-bond donation pattern involving the OH group of compound **3** was observed in the docking pose of this ligand into the binding site of the homomeric rat  $\alpha 7$  nAChR, with an orientation analogous to the one observed in Ac and Bt, as shown in Fig. 4. Ser-36 of the complementary face, a residue close in space to Ala-163, Asp-164, and Ile-165, accepts the hydrogen-bond donated by the ligand OH group.

## 2.2. Rational design of novel $\alpha 7$ nicotinic receptor ligands

Ulens et al. have demonstrated that docking-based virtual screening using AChBP crystal structure as target can successfully

**Table 3**  
Glide XP terms for designed compounds.

Compound	Rat $\alpha 7$ $K_i$ (nM)	Glide score	Rotable bond penalty (Kcal/mol)	Hydroph enclosure rewards (Kcal/mol)	$\pi$ -cation rewards (Kcal/mol)
<b>2f</b>	58	-11.87	0.09	-2.55	-3.07
<b>2e</b>	77	-11.79	0.06	-2.28	-3.16
<b>2c</b>	87	-11.31	0.08	-2.38	-2.91
<b>3b</b>	120	-10.57	0.09	-2.40	-3.00
<b>2a</b>	140	-11.79	0.10	-2.05	-3.01
<b>2g</b>	150	-12.14	0.10	-2.48	-3.05
<b>3d</b>	290	-11.25	0.11	-2.40	-3.45
<b>3</b>	420	-9.40	0.18	-1.83	-2.03

lead to the identification of novel  $\alpha 7$  nAChR ligands [21]. More recently, using a dataset mainly comprised of quinuclidine-containing compounds, de Kloe et al. have shown that a strong correlation exists between binding affinities for  $\alpha 7$  and AChBP-Ls and to a significantly lesser extent, to AChBP-Ac [26]. We have herein shown that a hydrogen bond donor feature observed to be important for binding affinity of anabaseine analogs to AChBP by interacting with this protein F-loop can also act in a similar manner in the binding pocket of the  $\alpha 7$  nAChR. Therefore, we reasoned that quinuclidine analogs containing a hydrogen bond donor functional group separated from the cationic center by a distance within the distance constraint range shown in Fig. 4 (13.6–20.9 Å) could satisfy the pharmacophoric requirements for binding to the  $\alpha 7$  protein. We accordingly designed a library of spirodiazepine and spiroimidazole quinuclidines and predicted their binding affinity to rat  $\alpha 7$ , using molecular docking as described herein. The synthetic scheme of the 14 compounds made is shown in Scheme 1.

Experimentally-observed binding data of the designed compounds are shown in Table 2. Results indicate that while all the designed compounds do not interact with the  $\alpha 4\beta 2$  subtype, compounds **3a**, **3b** and **3d**, which contain hydrogen-bond donors interact with  $\alpha 7$  nAChR with  $K_i$  less than 300 nM, and so do compounds **2a** through **2g**, which might tautomerize into lactim. Substitution within the aromatic ring of compounds **2a–g** slightly affects interaction with the receptor, while potential conjugation of the aromatic ring and azomethine moiety provide  $\pi$ - $\pi$  interaction. Compound **3a** ( $\alpha 7$  nAChR  $K_i$  7.2 nM) exhibited better binding affinity for  $\alpha 7$  than compounds **2** ( $\alpha 7$  nAChR  $K_i$  1500 nM) and compound **3** ( $\alpha 7$  nAChR  $K_i$  420 nM), and demonstrated partial agonism with an  $E_{max}$  of  $53.0 \pm 4.4\%$  and an  $EC_{50}$  of  $0.6 \pm 0.5 \mu\text{M}$ , by patch-clamp electrophysiology in rat  $\alpha 7$  nAChR [28]. Under the same experimental conditions, compound **3b** ( $\alpha 7$  nAChR  $K_i$  120 nM) had an  $E_{max}$  of  $22.0 \pm 4.7\%$  and an  $EC_{50}$  of  $1.2 \pm 0.7 \mu\text{M}$ . Functional data for compound **3** ( $\alpha 7$  nAChR  $E_{max}$  of  $77.00 \pm 0.02\%$  and  $EC_{50}$  of  $1.6 \pm 0.02 \mu\text{M}$ ) have been already reported in the literature [29]. For comparison, compounds **2h**, **2i**, **3c**, **3e**, lacking a hydrogen-bond donor satisfying the required distance constraint, do not demonstrate any interaction with  $\alpha 7$  nAChR. Fig. 5a–b illustrate the predicted binding mode of compounds **2b** and **3b** into the rat  $\alpha 7$  protein binding site, as derived from docking. We find that the OH group of the lactim form of compound **2b** donates a hydrogen-bond to Gln-57, whereas its methoxy oxygen atom accepts a hydrogen-

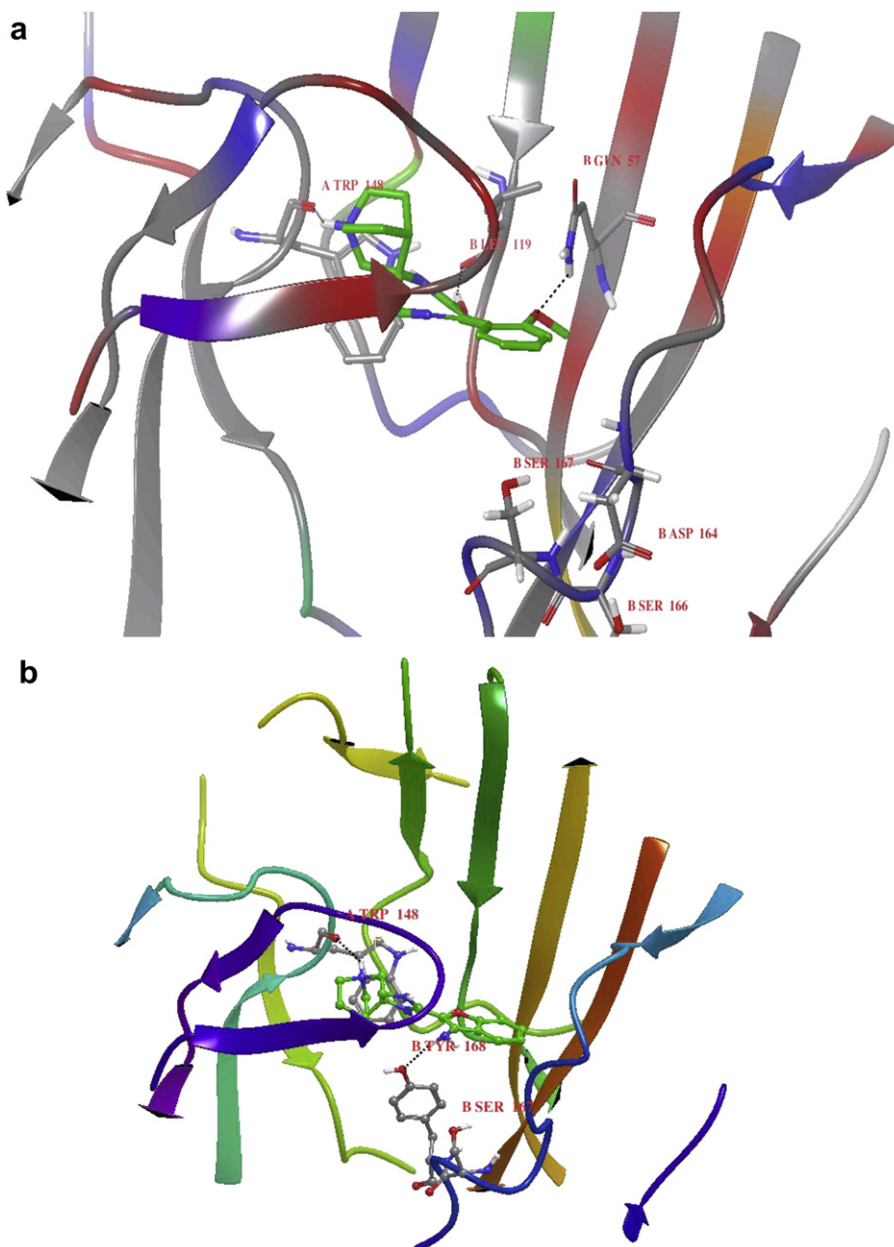


**Fig. 5.** a. Designed compound **2b** (in its lactim form) docked into rat  $\alpha 7$  homology model, is shown in green. The ligand OH group donates a hydrogen-bond to the backbone carbonyl oxygen atom of Leu-119 (in the complementary face), while its methoxy group accepts a hydrogen bond from Gln-57 (in the complementary face). Also shown are neighboring amino-acid side chains such as Ser-167, Ser-16, and Asp-164. The cationic center donates to the backbone CO group of Trp-148, in the principal face. All the three hydrogen-bond distances are shown in broken black lines. b. Designed compound **3b** docked into rat  $\alpha 7$  homology model. The ligand OH group donates a hydrogen-bond to Tyr-168 (in the complementary face), which is located in the F-loop (shown in dark blue). Also shown is neighboring amino-acid side chain, Ser-167. The cationic center donates to the backbone CO group of Trp-148, in the principal face. Both hydrogen-bond distances are shown in broken black lines.

bond from the backbone NH group of Leu-119, as shown in Fig. 5a. The  $\text{NH}_2$  group of compound **3b** donates a hydrogen-bond to the OH group of Tyr-168, a residue located in the F-loop region, as shown in Fig. 5b.

After docking in SP mode, the resulting best poses were subsequently docked in XP mode. The results thus obtained, shown in Table 3, indicate that the designed compounds are predicted to bind tighter than compound **3**, as Glide scores of the former are more negative than the Glide score of the latter. The results also illustrate that the best scoring conformations of the designed compounds which were successfully docked exhibit tighter hydrophobic enclosures [30,31] and cation- $\pi$  interactions, as

compared to compound **3**. This results in an increase in binding affinity. Furthermore, the XP-derived rotatable bond penalty appears to linearly correlate with rat  $\alpha 7$   $K_i$ , with an  $r^2$  value of 0.85 (Fig. 6). This finding indicates that the reduced flexibility of designed compounds, as compared to compound **3**, also contributes to improve binding affinity [32].

The use of AChBP crystal structures as surrogates for predicting binding of these novel spirodiazepines and spiroimidazolines to  $\alpha 7$  protein has also been investigated, by comparing the trend in docking score to the actually observed  $K_i$  data. With respect to the ability of the molecular docking to top-rank active  $\alpha 7$  compounds, the ROC scores obtained were low in all cases, varying from 0.51 to

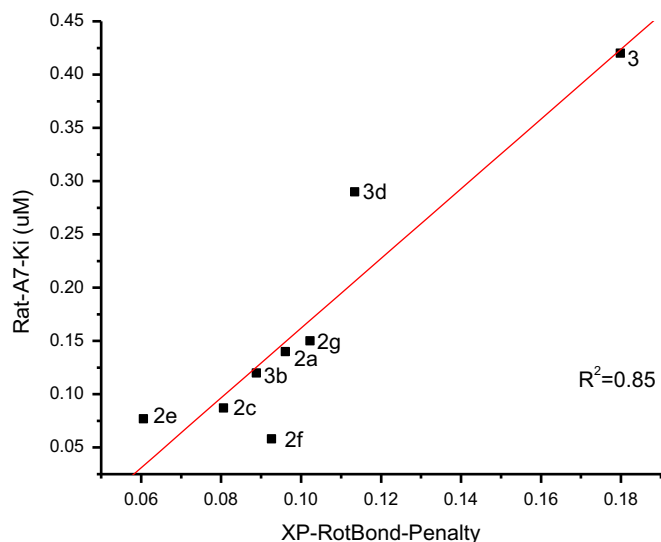


**Fig. 6.** Rat  $\alpha 7$  Ki highly correlates with XP-derived rotatable bond penalty, indicating that the more rigid the compound, the better the binding affinity.

0.62, as shown in Table 4. Of particular interest, however, is that using a rat  $\alpha 7$  homology model in docking did not score better (accuracy of 0.55) than the use of the original AChBP crystal structure templates. On average, when the validation set is also included, docking into Ls binding site scores the highest, followed by docking into the  $\alpha 7$  homology model.

The RMSD table derived from superimposing the crystal structure of Ac, Bt, and Ls is shown in Table 5. Examination of this table indicate that Ls is structurally more similar to Bt (rmsd = 1.6 Å) than to Ac (rmsd = 2.2 Å). This result is consistent with the finding that the weighted average value of roc score obtained in Table 4 for Ls protein (0.76) is closer to the one obtained with Bt protein (0.71) as compared to the one derived from docking into Ac protein (0.53).

### 3. Discussion and conclusions

We have carried out docking studies for a homologous series of benzylidene anabaseine analogs, for which crystallographic information on two of the analogs (**2** and **3**, Table 1) are available. These efforts are aimed at providing a more comprehensive understanding of the molecular basis of their interactions with nAChRs, which may aid in designing better drug candidates. Docking of benzylidene anabaseine analogs using Glide software accurately reproduces both experimentally-observed binding modes of DMXBA and of its metabolite, in the binding pocket of Ac. Similar docking poses of anabaseine analogs bound to Bt, Ls and  $\alpha 7$  nAChR, respectively, have been derived. These results support the importance of the hydrogen bond donor feature in the ligand, as described previously by Talley et al. [24] and Hibbs et al. [17]. As

**Table 4**

ROC accuracy of docking in ranking the binding of ligands to rat  $\alpha 7$  protein. X-ray crystal structures of AChBPs and  $\alpha 7$  homology model were used for docking, as described in the methods section.

Protein system	Validation set (N = 493)	Designed set (N = 14)	Weighted average Roc score
Ac	0.53	0.62	0.53
Bt	0.72	0.51	0.71
Ls	0.77	0.62	0.76
$\alpha 7$	0.74	0.55	0.73

**Table 5**

RMSD table (expressed in Å) obtained from superimposing the crystal structures of Ac, Bt, and Ls proteins. The pdb codes used are 2byq, 2bj0, and 2byq, respectively.

Protein system	Ac	Bt	Ls
Ac	0	2.2	1.9
Bt		0	1.6
Ls			0

observed experimentally by Taylor and coworkers [17], our docking studies highlight the importance of the D-SS (Asp-164, Ser-166, Ser-167) amino acid residues triad from the complementary face of Ac, which interacts via a hydrogen bonding network with the benzylidene 4-position substituent. This was also found in docking poses for the Bt protein, but in this case stabilization appears to occur via a hydrogen bonding network with Glu-163 and Tyr-164, located in the same complementary face region. While the same amino acid residue motif is found in the Ls protein, i.e., Glu-163 and Tyr-164, we have not observed a similar docking pose for compounds **3** and **4**, in this protein. Instead, we have found a low-energy pose in which the ligand hydroxyl group at the 4-position in this case accepts a hydrogen-bond from Gln-73 of the complementary face, while the oxygen atom of the methoxy group at the 2-position accepts a hydrogen-bond from Tyr-192 of the principal face, as shown in Fig. 3. Such an alternative binding mode results from a rotation of approximately 90° about an axis passing through the ligand basic nitrogen atom and perpendicular to the indole side-chain of the conserved Trp-143. This pose, while reminiscent of “conformation B” observed in the co-crystal structure of compound **2** complexed with Ac (Fig. S2), represents a greater displacement of the benzylidene region of the ligand.

Docking observations, at least in part help to explain the significant loss of affinities for DMXBA (compound **2**) vs. that for the 4-OH metabolite (compound **3**). For Bt, loss of the hydrogen bond donor capacity (OH to OCH<sub>3</sub>) leads to slight (2.5 fold) decrease in  $K_d$  value. But for Ac, with a more hydrophilic amino acid residue environment in the same complementary face region, the loss in affinity is much more dramatic (110-fold). In the case of Ls, in order to probe whether OH group at position 4 acts as a better hydrogen-bond acceptor than OCH<sub>3</sub>, we have carried out a quantum mechanical calculation of atom polarization in the binding site, using Maestro QPLD protocol [33]. Results indicated that the oxygen atom in the OH group at position 4 of benzylidene anabaseine was more negatively charged ( $q = -0.55$ ) than in the methoxy group ( $q = -0.37$ ), suggesting that compound **3** might be a better hydrogen bond acceptor than compound **2**.

Docking results obtained for anabaseine analogs are consistent with the historical nicotinic cholinergic pharmacophore models [1]. The pyridine nitrogen atom acts as hydrogen bond acceptor, while the pyridine ring, itself, fits the required hydrophobic aromatic feature. Anabaseine congeners containing OH and NH<sub>2</sub> functional groups additionally donate a hydrogen-bond, (or accept one as shown by docking into Ls binding site), which may explain the fact that such analogs bind the strongest in this series of compounds [24]. The ligand-protonated nitrogen and the OH group at position-4 and at position-2, are separated by a distance of 8.94 Å and 5.05 Å, respectively. It is important to mention that these interfeature distances are consistent with the distances of about 12 Å and 5.5 Å between the carbonyl oxygen atom of the quintessential conserved Trp and the side-chain oxygen atom of Asp-164 (or Tyr-164) in the F-loop and of Tyr-192, respectively, in the docked poses for Bt (Fig. 2), Ac, and Ls. This result suggests a lock and key model of molecular recognition. Exception is found, however, with rat  $\alpha 7$  model binding site where the side-chain oxygen atom of Asp-164 is separated from the carbonyl oxygen atom of the conserved Trp by

a distance of about 19.4 Å. Not surprisingly, Ser-36, which is separated from the conserved Trp by a 12.9 Å distance, interacts with the ligand OH group at 4-position, in the docked poses (Fig. 4).

Docking results obtained for the designed compounds, shown in Fig. 5a, suggest that the lactim form of spirodiazepine analogs might interact with the rat  $\alpha 7$  protein by adopting a “conformation B-like” binding mode of DMXBA into the Ac protein, as also shown in Fig. S2. The ligand OH group donates a hydrogen bond to the backbone carbonyl oxygen atom of Leu-119, while its methoxy group accepts a hydrogen bond from the amide side-chain group of Gln-57, located in the complementary face. By contrast, a designed spiroimidazoline containing a hydrogen-bond donor group at the appropriate location, shown in Fig. 5b, might interact with the rat  $\alpha 7$  protein by adopting a “conformation A-like” binding mode of DMXBA into the Ac protein, as also illustrated in Fig. S1.

In addition to hydrogen-bond interactions that have been widely discussed herein, and the more commonly observed interactions such as van der Waals, columbic and pairwise lipophilic, Glide XP has revealed the importance of hydrophobic enclosures, cation- $\pi$  interactions, and loss of configurational entropy in contributing to the gain in binding affinity observed for the novel spirodiazepine and spiroimidazoline quinuclidine analogs (Table 3 and Fig. 6). These additional and important interactions also contribute to the binding of benzylidene anabaseine analogs to AChBPs, as shown in Table S1. However, the fact that active compounds such as **3a**, **2b** and **2d** were not well docked in XP mode after being successfully docked in SP mode, suggests that significant work to account for receptor flexibility is still needed in order to improve the accuracy of available docking packages.

As shown in Table 4, a comparison of Roc scores derived from docking ligands into AChBPs crystal structures, in order to predict ligand binding to rat  $\alpha 7$ , suggests that the best results have been obtained with Ls, followed by the rat  $\alpha 7$  homology model. On average, poorest results were obtained when using Ac model, which appear to be the most structurally dissimilar to both its counterparts Bt and Ls, as can be seen from the rmsd values shown in Table 5. These findings are in agreement with the work of de Kloe et al. which has recently shown that a strong correlation exists between binding affinities for  $\alpha 7$  and AChBP-Ls and to a significantly lesser extent, to AChBP-Ac [26]. In the light of the results discussed above, we suggest that Ls crystal structure may be a better template to use in developing an homology model for rat  $\alpha 7$ , as compared to Bt and Ac crystal structures. Moreover, Ls or Bt protein may also be a better choice for designing an AChBP/rat  $\alpha 7$  chimera protein. It will also be of interest to ascertain whether differences in ring orientation are evident in the fluorescence quantum yield, emission shifts and difference absorption spectra of the substituted anabaseines in a complex with the *Bulinus* and *Lymnaea* species.

In conclusion, we have used molecular docking to study the interactions of benzylidene anabaseine congeners with AChBPs and rat  $\alpha 7$  nAChR. We have found that binding affinity is primarily mediated via electrostatic interactions (hydrogen-bond,  $\pi$ -cation and  $\pi$ - $\pi$ ), pairwise lipophilic, hydrophobic enclosures and loss of configurational entropy as well. In particular, a hydrogen bond donor feature appears to contribute to ligand binding to Ac, Bt and  $\alpha 7$  nAChR. Docking of compounds **3** and **4** into the ligand binding pocket of Ls shows the ligand OH group acting as hydrogen-bond acceptor, instead. The use of AChBP as surrogate to design novel spirodiazepines and spiroimidazolines quinuclidines which bind  $\alpha 7$  nAChR has been investigated. Here the aza nitrogen in the bicycle ring system takes the place of the cyclic imine nitrogen in protonating, to be the hydrogen bond donor. A restriction in ligand motion upon binding also appears to contribute to the increase in binding affinity observed for the designed compounds. On the

whole, the results obtained show that models derived from Ls exhibits the highest accuracy in predicting ligand binding to rat  $\alpha 7$  protein. These findings may have implications in selecting the best template to use in building an homology model for nAChR or a chimera AChBP/nAChR. It is important to notice that in this specific case of docking, the use of a validated homology model didn't add significant value, as compared to the simple use of the template protein. Experimental data have shown that the designed novel compounds selectively bind to rat  $\alpha 7$  nAChR. In particular, compound **3a** binds  $\alpha 7$  nAChR with a much better affinity than both DMXBA (compound **2**) and its active 4-OH metabolite (compound **3**), and demonstrates partial agonism.

## 4. Experimental section

### 4.1. Molecular docking of ligands into AChBPs

Docking studies were carried out using Glide 5.5 [34–36]. Protein structures were prepared using Maestro protein preparation wizard. Following hydrogen-bonding assignment optimization, water molecule orientations were exhaustively sampled, and the protein-ligand complexes were energy-minimized until an rmsd of 0.30 Å was reached. To validate the docking procedure, a self-docking of the crystallized ligands into their cognate AChBP protein was carried out. Validation studies were carried out using co-crystal structures with the following pdb codes: 1uw6 (Ls in complex with nicotine) [15], 2bj0 (Bt in complex with CAPS, i.e. 3-(cyclohexylamino)-1-propanesulfonic acid) [16], and 2wn9 (Ac in complex with 2-Methoxy-4-OH benzylidene anabaseine, called compound **3** herein) [17]. A docking grid was constructed for each protein by using the centroid of the bound ligand and a maximum size of 20 Å. Flexibility of OH groups for amino acid side chains at the binding site was allowed. Crystallographic water molecules at each binding site were included. To mimic the quintessential hydrogen bond involving Trp-147 (Ac) carbonyl oxygen and the ligand-protonated nitrogen, experimentally observed in the crystal structures of anabaseine DMXBA (compound **2** in Table 1), and 2-MeO, 4-OHBA (compound **3** in Table 1), bound to Ac [17], an H-bond constraint was accordingly specified. To mimic flexibility of the protein structure, a scaling of van der Waals radii for non-polar parts in the binding site and the ligands was carried out. Best docked poses derived in SP mode were subsequently re-docked in XP mode. The Glide XP visualizer module [34], was used to visualize and analyze the derived docking poses.

### 4.2. Homology modeling of the $\alpha 7$ nAChR

Three-dimensional models of the extracellular domain of the rat  $\alpha 7$  protein were obtained from comparative modeling using spatial restraints, as implemented within Discovery Studio, using MODELLER [37–39]. The three-dimensional structure of AChBP from Ls complexed with nicotine (pdb code 1uw6) was used as template. The derived protein structures were validated with regard to protein structure architecture and stereochemistry using the protein analysis programs Procheck [40], and Verify\_3D [41], as implemented within the UCLA DOE web server [42]. Procheck results showed that 86% of residues were found in the most-favored region of the Ramachandran plot, and Verify\_3D results indicated that 77.4% of the residues had an averaged 3D-1D score >0.2. Further refinement of the models was carried out within Maestro (Schrodinger, Inc.) protein preparation module, prior to any docking simulation. In addition, biochemical validation of the  $\alpha 7$  homology model was carried out by docking a diverse chemical library of 493 compounds of known binding affinity to the  $\alpha 7$  nAChR. The dataset, extracted from an in-house compound

collection, was comprised of 127 actives ( $\alpha 7 K_i \leq 500$  nM) and 366 decoys ( $\alpha 7 K_i > 500$  nM). The performance of the docking exercise to classify compounds with respect to their binding affinity using this homology model was evaluated by means of the area under the receiver operating characteristic (ROC) curve. The accuracy obtained was 0.74. Note that an area of 0.50 indicates random performance, while an area of 1.00 indicates a perfect model.

#### 4.3. Chemistry

Unless otherwise stated, all reactions were carried out under a nitrogen atmosphere, using commercially available anhydrous solvents. NMR spectra were carried out on a Varian 300 in the solvents specified. HPLC purity determinations were carried out using a Phenomenex C18 100 mm  $\times$  4.6 mm column with 5  $\mu$ m particle size; gradient: 97.5–2.5% A, 1 mL/min flow rate (A, 0.05% trifluoroacetic acid in H<sub>2</sub>O; B, 0.05% trifluoroacetic acid in acetonitrile). All test compounds were confirmed to be >95% pure by HPLC and high resolution LCMS.

##### 4.3.1. 5-Phenylspiro[1,3-dihydro-1,4-diazepine-2,3'-quinuclidine]-7-ol (**2a**)

This procedure illustrates the general method for preparation of **2a–g**. 3-Amino-3-(aminomethyl)quinuclidine (**1**) (75 mg, 0.5 mmol) and ethyl benzoylacetate (100 mg, 0.5 mmol) were dissolved in *i*-butanol (3 ml). The reaction mixture was heated at 100 °C overnight, cooled to ambient temperature and concentrated. The residue was purified by preparative HPLC to yield **2a** trifluoroacetate (105 mg, 53%). <sup>1</sup>H NMR (CD<sub>3</sub>OD, 300 MHz)  $\delta$  8.07 (d, 2H), 7.72 (m, 1H), 7.60 (m, 2H), 4.23 (dd, 2H, *J* = 65, 12 Hz), 3.94 (dd, 2H, *J* = 28, 10 Hz), 3.59–3.38 (m, 6H), 2.49 (s, 1H), 2.35–2.10 (m, 4H). High resolution LSMS, *m/e* 284.1767, C<sub>17</sub>H<sub>22</sub>N<sub>3</sub>O, calc. 284.1763.

##### 4.3.2. 5-(2-Methoxyphenyl)spiro[1,3-dihydro-1,4-diazepine-2,3'-quinuclidine]-7-ol (**2b**)

High resolution LCMS *m/e* 314.1869, C<sub>18</sub>H<sub>24</sub>N<sub>3</sub>O<sub>2</sub>, calc. 314.1869.

##### 4.3.3. 5-(4-Methoxyphenyl)spiro[1,3-dihydro-1,4-diazepine-2,3'-quinuclidine]-7-ol (**2d**)

High resolution LCMS *m/e* 314.1882, C<sub>18</sub>H<sub>24</sub>N<sub>3</sub>O<sub>2</sub>, calc. 314.1869.

##### 4.3.4. 5-(2-Furyl)spiro[1,3-dihydro-1,4-diazepine-2,3'-quinuclidine]-7-ol (**2g**)

High resolution LCMS *m/e* 274.1553, C<sub>15</sub>H<sub>20</sub>N<sub>3</sub>O<sub>2</sub>, calc. 274.1556.

##### 4.3.5. 6-phenylspiro[1,3-dihydro-1,4-diazepine-2,3'-quinuclidine] (**2h**)

3-Amino-3-(aminomethyl)quinuclidine (**1**) (75 mg, 0.5 mmol) and [3-(dimethylamino)-2-phenylprop-2-enylidene]-dimethylammonium hexafluorophosphate (100 mg, 0.4 mmol) were dissolved in methanol (5 ml). The reaction mixture was refluxed overnight and concentrated. The residue was purified by preparative HPLC to yield **2h** trifluoroacetate (75 mg, 20%). <sup>1</sup>H NMR (CD<sub>3</sub>OD, 300 MHz)  $\delta$  0.15 (s, 1H), 8.01 (s, 1H), 7.52–7.38 (m, 5H), 4.50 (d, 1H, *J* = 12 Hz), 3.73 (dd, 2H, *J* = 27, 12 Hz), 3.60–3.38 (m, 5H), 2.22–1.98 (m, 5H).

##### 4.3.6. 6-Phenylspiro[1,4-diazepane-2,3'-quinuclidine]-5,7-dione (**2i**)

A mixture of 3-amino-3-(aminomethyl)quinuclidine (**1**) (75 mg, 0.5 mmol) and diethyl 2-phenylmalonate (118 mg, 0.5 mmol) were heated at 150 °C in microwave for 5 min. The reaction mixture was cooled to r.t. and purified by preparative HPLC to yield **2i** trifluoroacetate (98 mg, 24%). <sup>1</sup>H NMR (CD<sub>3</sub>OD, 300 MHz)  $\delta$  7.46–7.22 (m, 5H), 4.30 (s, 1H), 4.02 (dd, 2H, *J* = 50, 13 Hz), 3.53 (dd, 2H, *J* = 53,

12 Hz), 3.53–3.15 (m, 4H), 2.23–1.98 (m, 5H). High resolution LCMS *m/e* 300.1723, C<sub>17</sub>H<sub>22</sub>N<sub>3</sub>O<sub>2</sub>, calc. 300.1712.

##### 4.3.7. 2-(3-Hydroxybenzofuran-2-yl)spiro[1,5-dihydroimidazole-4,3'-quinuclidine] (**3a**)

A mixture of 3-amino-3-(aminomethyl)quinuclidine (**1**) (75 mg, 0.5 mmol), methyl 2-(cyanomethoxy)benzoate (96 mg, 0.5 mmol) and one drop of carbon disulfide was heated in a sealed vial at 100–110 °C overnight. The reaction mixture was cooled to r.t. and purified by preparative HPLC to yield **3a** trifluoroacetate (98 mg, 48%). <sup>1</sup>H NMR (CD<sub>3</sub>OD, 300 MHz)  $\delta$  7.98 (d, 1H), 7.65 (m, 2H), 7.43 (m, 2H), 4.26 (dd, 2H, *J* = 76, 12), 3.77 (dd, 2H, *J* = 35, 14), 3.60–3.38 (m, 4H), 2.50–2.33 (m, 2H), 2.15 (m, 3H).

##### 4.3.8. 2-(3-Aminobenzofuran-2-yl)spiro[1,5-dihydroimidazole-4,3'-quinuclidine] (**3b**)

A mixture of 3-amino-3-(aminomethyl)quinuclidine (**1**) (75 mg, 0.5 mmol), (2-cyanophenoxy)acetonitrile (79 mg, 0.5 mmol) and one drop of carbon disulfide was heated in a sealed vial at 100–110 °C overnight. The reaction mixture was cooled to r.t. and purified by preparative HPLC to yield **3b** trifluoroacetate (145 mg, 68%). <sup>1</sup>H NMR (CD<sub>3</sub>OD, 300 MHz)  $\delta$  7.96 (d, 1H), 7.64 (t, 1H), 7.50 (d, 1H), 7.36 (t, 1H), 4.20 (dd, 2H, *J* = 60, 12 Hz, 2H), 3.79 (dd, 2H, *J* = 22, 12 Hz, 2H), 3.63–3.38 (m, 4H), 2.42 (m, 2H), 2.17 (m, 3H). High resolution LCMS *m/e* 290.1707, C<sub>17</sub>H<sub>21</sub>N<sub>4</sub>O, calc. 290.1715.

##### 4.3.9. 2-Phenylspiro[1,5-dihydroimidazole-4,3'-quinuclidine] (**3c**)

A mixture of 3-amino-3-(aminomethyl)quinuclidine (**1**) (475 mg, 3.0 mmol) and methyl benzimidate hydrochloride (602 mg, 3.5 mmol) in methanol (3 ml) was heated in microwave at 150 °C for 5 min. The reaction mixture was concentrated *in vacuo*. The residue was purified by preparative HPLC to yield **3c** (0.3 g, 28%). <sup>1</sup>H NMR (CD<sub>3</sub>OD, 300 MHz)  $\delta$  8.00 (d, 2H), 7.85 (m, 1H), 7.69 (m, 2H), 4.33 (dd, 2H, *J* = 75, 11), 3.80 (dd, 2H), 3.59–3.37 (m, 4H), 2.59–2.40 (m, 2H), 2.09 (m, 3H). High resolution LCMS *m/e* 242.1649, C<sub>15</sub>H<sub>20</sub>N<sub>3</sub>, calc. 242.1657.

##### 4.3.10. 2-Spiro[1,5-dihydroimidazole-4,3'-quinuclidine]-2-ylphenol (**3d**)

3-Amino-3-(aminomethyl)quinuclidine (**1**) (75 mg, 0.5 mmol) and 4-hydroxycoumarin (81 mg, 0.5 mmol) were dissolved in *i*-butanol (3 ml). The reaction mixture was heated at 100 °C overnight, cooled to ambient temperature and concentrated. The residue was purified by preparative HPLC to yield **3d** trifluoroacetate (15 mg, 8%). <sup>1</sup>H NMR (CD<sub>3</sub>OD, 300 MHz)  $\delta$  7.88 (d, 1H), 7.66 (m, 1H), 7.12 (m, 2H), 4.29 (dd, 2H, *J* = 79, 10), 4.78 (dd, 2H), 3.56–3.37 (m, 4H), 2.50–2.33 (m, 2H), 2.16 (m, 3H).

##### 4.3.11. 2-Spiro[1,5-dihydroimidazole-4,3'-quinuclidine]-2-ylbenzo[b]furan (**3e**)

Compound (**3e**) was prepared from 3-amino-3-(aminomethyl)quinuclidine (**1**) and methyl benzofurancarboximidate hydrochloride according to procedure for **3c**. <sup>1</sup>H NMR (CD<sub>3</sub>OD, 300 MHz)  $\delta$  8.12 (s, 1H), 7.88 (d, 1H), 7.74 (d, 1H), 7.66 (t, 1H), 7.48 (t, 1H), 4.36 (dd, 2H, *J* = 75, 10), 3.81 (dd, 2H), 3.62–3.38 (m, 4H), 2.58–2.40 (m, 2H), 2.18 (m, 3H). High resolution LCMS *m/e* 351.1821, C<sub>20</sub>H<sub>23</sub>N<sub>4</sub>O<sub>2</sub>, calc. 351.1821.

#### 4.4. Competition binding to receptors in membrane preparations

Binding assays to membrane bound nicotinic receptors were carried out using standard methods adapted from published procedures [43,44]. In brief, membranes were reconstituted from frozen stocks and incubated for 2 h in 150  $\mu$ l assay buffer (PBS) in the presence of competitor compound (0.001 nM–100  $\mu$ M) and radioligand. [<sup>3</sup>H]-methyllycaconitine ([<sup>3</sup>H]-MLA, Perkin–Elmer Life

Sciences) was used for  $\alpha 7$  binding studies on rat hippocampal membranes and [ $^3\text{H}$ ]-epibatidine (Perkin–Elmer Life Sciences) was used for binding studies at the  $\alpha 4\beta 2$  on rat cortical membranes, ganglion-type nicotinic receptors on SH-SY5Y cellular membranes and muscle-type nicotinic receptors on TE-671 cellular membranes. Incubation was terminated by rapid filtration on a multimanifold tissue harvester (Brandel, Gaithersburg, MD) using GF/B filters presoaked in 0.33% polyethyleneimine (w/v) to reduce non-specific binding. Filters were washed 3 times with ice-cold PBS and retained radioactivity was determined by liquid scintillation counting.

#### 4.5. Binding data analysis

Single-point binding data was determined at a competitor concentration of 5  $\mu\text{M}$  and are expressed as the percent inhibition of control radioligand binding. For  $\text{IC}_{50}$  determinations, replicates for each point of a seven-point dose–response curve were averaged and plotted against the log of drug concentration.  $\text{IC}_{50}$  values (concentration of the compound that produces 50% inhibition of binding) were determined by least squares non-linear regression using GraphPad Prism software (GraphPAD, San Diego, CA).  $K_i$  values were calculated using the Cheng–Prusoff equation [45].

#### Acknowledgment

We sincerely thank Dr Gary Byrd for high resolution LCMS and Christopher Helper for binding affinity studies. We also thank Merouane Bencherif, Craig Miller, and Heather Savelle for helpful discussions, suggestions and comments.

#### Appendix. Supplementary material

Supplementary data associated with this article can be found, in the online version, at doi:10.1016/j.ejmech.2011.09.033.

#### References

- [1] M.N. Romanelli, P. Gratteri, L. Guanalini, E. Martini, C. Bonaccini, F. Gualtieri, *Chem. Med. Chem.* 2 (2007) 2–24.
- [2] S. Breining, *Curr. Top. Med. Chem.* 4 (2004) 609–629.
- [3] J.D. Schmitt, *Curr. Med. Chem.* 7 (2000) 749–800.
- [4] C. Conejero-Goldberg, P. Davies, L. Ulloa, *Neurosci. Biobehav. Rev.* 32 (2008) 693–706.
- [5] A. Mazurov, T. Hauser, C.H. Miller, *Curr. Med. Chem.* 13 (2006) 1567–1584; Erratum in, *Curr. Med. Chem.* 14 (2007) 1593.
- [6] J.W. Daly, *Cell. Mol. Neurobiol.* 25 (2005) 513–552.
- [7] A. Taly, P.J. Corringier, D. Guedin, P. Lestage, J.P. Changeux, *Nat. Rev. Drug Discov.* 8 (2009) 733–750.
- [8] K.B. Mihalak, F.I. Caroll, C.W. Luetje, *Mol. Pharmacol.* 70 (2006) 801–805.
- [9] J.W. Coe, P.R. Brooks, M.G. Vetelino, M.C. Wirtz, E.P. Arnold, J. Huang, S.B. Sands, T.I. Davis, L.A. Lebel, C.B. Fox, A. Shrikhande, J.H. Heym, E. Schaeffer, H. Rollema, Y. Lu, R.S. Mansbach, L.K. Chambers, C.C. Rovetti, D.W. Schulz, F.D. Tingley, B.T. O'Neill, *J. Med. Chem.* 48 (2005) 3474–3477.
- [10] [www.Clinicaltrials.gov](http://www.Clinicaltrials.gov).
- [11] Targacept announces positive top-line results from phase 2 trial of TC-5619 in cognitive dysfunction in schizophrenia. Press release, 01/21/2011, Winston-Salem, NC, USA.
- [12] K. Brejc, W.J. van Dijk, R.V. Klaassen, M. Schurmans, J. van de Oost, A.B. Smit, T.K. Sixma, *Nature* 411 (2001) 269–276.
- [13] N. Unwin, *J. Mol. Biol.* 346 (2005) 967–989.
- [14] Y. Bourne, T.T. Talley, S.B. Hansen, P. Taylor, P. Marchot, *EMBO J.* 24 (2005) 1512–1522.
- [15] P.H. Celie, S.E. Rossum-Fikkert, W.J. van Dijk, K. Brejc, A.B. Smit, T.K. Sixma, *Neuron* 41 (2004) 907–914.
- [16] P.H. Celie, R.V. Klaassen, S.E. van Rossum-Fikkert, R. van Elk, P. van Nierop, A.B. Smit, T.K. Sixma, *J. Biol. Chem.* 280 (2005) 26457–26466.
- [17] R.E. Hibbs, G. Sulzenbacher, J. Shi, T.T. Talley, S. Conrod, W.R. Kem, P. Taylor, P. Marchot, Y. Bourne, *EMBO J.* 28 (2009) 3040–3051.
- [18] S. Mecozzi, A.P. West, D.A. Dougherty, *Proc. Natl. Acad. Sci. USA* 93 (1996) 10566–10571.
- [19] J.D. Schmitt, C.G. Sharples, W.S. Caldwell, *J. Med. Chem.* 42 (1999) 3066–3074.
- [20] D.A. Dougherty, *J. Org. Chem.* 16 (2008) 3667–3673.
- [21] C. Ullens, A. Akdemir, A. Jongejan, R. van Elk, S. Bertrand, A. Perrakis, R. Leurs, A.B. Smit, T.K. Sixma, D. Bertrand, I.J.P. de Esch, *J. Med. Chem.* 52 (2009) 2372–2383.
- [22] R.L. Papke, E.M. Meyer, S. Lavieri, S.R. Bollompally, T.A. Papke, N.A. Horenstein, Y. Itoh, J.K. Porter Papke, *Neuropharmacol.* 46 (2004) 1023–1038.
- [23] C. Stokes, J.K. Papke, N.A. Horenstein, W.R. Kem, T.J. McCormack, R.L. Papke, *Mol. Pharmacol.* 66 (2004) 14–24.
- [24] T.T. Talley, S. Yalda, K.-Y. Ho, Y. Tor, F.S. Soti, W.R. Kem, P. Taylor, *Biochemistry* 45 (2006) 8894–8902.
- [25] S.H. Slavov, M. Radzivilovits, S. LeFrancois, I. Stoyanova-Slavova, F. Sot, W.R. Kem, A.R. Katritzky, *Eur. J. Med. Chem.* 45 (2010) 2433–2446.
- [26] G.E. De Kloe, K. Retra, M. Geitmann, P. Kallblad, T. Nahar, R. van Elk, A.B. Smit, J.E. van Muijlwijk-Koezen, R. Leurs, R.H. Irth, U.H. Danielson, I.J.P. de Esch, *J. Med. Chem.* 53 (2010) 7192–7201.
- [27] G. Mullen, J. Napier, M. Balestra, T. DeCory, G. Hale, J. Macor, R. Mack, J. Loch, E. Wu, A. Kover, P. Verhoest, A. Sampognaro, E. Phillips, Y. Zhu, R. Murray, R. Griffith, J. Blosser, D. Gurley, A. Machulskis, J. Zongrone, A. Rosen, J. Gordon, *J. Med. Chem.* 43 (2000) 4045–4050.
- [28] A.N. Placzek, F. Grassi, E.M. Meyer, R.L. Papke, *J. Med. Chem.* 68 (2005) 1863–1876.
- [29] W.R. Kem, V.M. Mahnir, L. Prokai, R.L. Papke, X. Cao, S. LeFrancois, K. Wildeboer, K. Prokai-Tatrai, J. Porter-Papke, F. Soti, *Mol. Pharmacol.* 65 (2004) 56–67.
- [30] T. R. Young, B. Abel, B.J. Kim, R.A. Berne Friesner, *Proc. Natl. Acad. Sci. USA* 104 (2007) 808–813.
- [31] R.A. Friesner, R.B. Murphy, M.P. Repasky, L.L. Frye, J.R. Greenwood, T.A. Halgren, P.C. Sanschagrin, D.T. Mainz, *J. Med. Chem.* 49 (2006) 6177–6196.
- [32] C.A. Chang, W. Chen, M.K. Gilson, *Proc. Natl. Acad. Sci. USA* 104 (2007) 1534–1539.
- [33] A.E. Cho, V. Guallar, B.J. Berne, R. Friesner, *J. Comp. Chem.* 26 (2005) 915–931.
- [34] Schrodinger, Inc., 101 SW Main Street, Suite 1300, Portland, OR 97204.
- [35] R.A. Friesner, J.L. Banks, R.B. Murphy, T.A. Halgren, J.J. Klicic, D.T. Mainz, M.P. Repasky, E.H. Knoll, M. Shelley, J.K. Perry, D.E. Shaw, *J. Med. Chem.* 47 (2004) 1739–1749.
- [36] T.A. Halgren, R.B. Murphy, R.A. Friesner, H.S. Beard, L.L. Frye, W.T. Pollard, J.L. Banks, *J. Med. Chem.* 47 (2004) 1750–1759.
- [37] Accelrys Inc., San Diego, CA, 2006.
- [38] N. Eswar, M.A. Marti-Renom, B. Webb, M.S. Madhusudhan, D. Eramian, M. Shen, U. Pieper, A. Sali, Comparative protein structure modeling with MODELLER, in: *Current Protocols in Bioinformatics*. John Wiley & Sons, Inc., 2006 Supplement 15, 5.6.1–5.6.30, 2006.
- [39] M.A. Marti-Renom, A. Stuart, A. Fiser, R. Sánchez, F. Melo, A. Sali, *Annu. Rev. Biophys. Biomol. Struct.* 29 (2000) 291–325.
- [40] R.A. Laskowski, M.W. MacArthur, D.S. Moss, J.M. Thornton, *App. Cryst* 26 (1993) 283–291.
- [41] D. Eisenberg, R. Luthy, J.U. Bowie, *Methods Enzymol.* 277 (1997) 396–404.
- [42] <http://www.doe-mbi.ucla.edu/SAVES/>.
- [43] P.M. Lippello, K.G. Fernandes, *Mol. Pharmacol.* 29 (1986) 448–454.
- [44] A.R. Davies, D.J. Hardick, I.S. Blagbrough, B.V. Potter, A.J. Wolstenholme, S. Wonnacott, *Neuropharmacol.* 38 (1999) 679–690.
- [45] Y. Cheng, W.H. Prusoff, *Biochem. Pharmacol.* 22 (1973) 3099–3108.